Pairing properties of semilocal coordinate- and momentum-space regularized chiral interactions

P. Yin,[1] X. L. Shang,[1,2,*] J. N. Hu,[3] J. Y. Fu,[1,2] E. Epelbaum,[4] and W. Zuo[1,2]

[1]*CAS Key Laboratory of High Precision Nuclear Spectroscopy, Institute of Modern Physics, Chinese Academy of Sciences, Lanzhou 730000, China*

[2]*School of Nuclear Science and Technology, University of Chinese Academy of Sciences, Beijing 100049, China*

[3]*School of Physics, Nankai University, Tianjin 300071, China*

[4]*Institut für Theoretische Physik II, Ruhr-Universität Bochum, D-44780 Bochum, Germany*

(Received 15 February 2023; revised 23 July 2023; accepted 22 August 2023; published 8 September 2023)

We investigate the pairing properties of state-of-the-art semilocal coordinate-space and semilocal momentum-space regularized chiral interactions. Specifically, we calculate the pairing gaps in the $^3SD_1$ channel of symmetric nuclear matter and in $^1S_0$ and $^3PF_2$ channels of pure neutron matter within the BCS approximation using these chiral interactions. We evaluate the truncation errors of chiral expansions of the pairing gaps with a Bayesian approach. We find overall weak regulator dependence and robust convergence from low to high densities for the $^3SD_1$ and $^1S_0$ pairing gaps, while we find chaotic behavior for the $^3PF_2$ results. We compare the converged results of the chiral interactions with the results of the Argonne v18 (Av18) potential. Their discrepancies in the $^3SD_1$ and $^3PF_2$ channels at high densities demonstrate that the nucleon-nucleon interactions in these two channels may need further constraints at high scattering energies. We have also investigated the effect of the tensor force on the $^3SD_1$ and $^3PF_2$ pairing gaps. The apparently different tensor force effects of the chiral interactions and the Av18 potential for the $^3SD_1$ and $^3PF_2$ pairing gaps indicate that the tensor components of these interactions are quite different.

DOI: 10.1103/PhysRevC.108.034002

I. INTRODUCTION

Nucleon-nucleon (*NN*) interaction, serving as the sole input of the *ab initio* nuclear many-body theory, plays a fundamentally significant role in nuclear physics. Chiral effective field theory (EFT) allows one to derive *NN* interactions based on the underlying fundamental quantum chromodynamics and provides a straightforward path to generate consistent and systematically improvable many-body interactions and exchange currents [1].

In Refs. [2,3], a set of semilocal coordinate-space (SCS) regularized chiral EFT *NN* interactions were developed up through the fifth chiral order (N^4LO) using a local regulator for the pion-exchange contributions, which allows one to substantially reduce finite-cutoff artifacts. In particular, the long-range contributions are regularized in coordinate space via $V_\pi(\vec{r}) \longrightarrow V_{\pi,R}(\vec{r}) = V_\pi(\vec{r})[1 - e^{-\frac{r^2}{R^2}}]^n$, where the cutoff R was chosen in the range of $R = 0.8$, 0.9, 1.0, 1.1, and 1.2 fm. The exponent n was set as $n = 6$, but choosing $n = 5$ or $n = 7$ led to a comparable description of the phase shifts [2]. For contact interactions, a nonlocal Gaussian regulator in momentum space was employed with the cutoff Λ being related to R via $\Lambda = 2/R$. These novel chiral EFT interactions have been successfully applied to *ab initio* calculations of nuclear structure, nuclear reactions, and nuclear matter [4–11]. However, the numerical implementation of the three-nucleon potentials with the coordinate-space regulator in the Faddeev and Yakubovsky equations appears to be challenging, in particular, as chiral order increases.

Therefore, a new generation of semilocal momentum-space (SMS) regularized chiral EFT *NN* interactions was developed in Ref. [12], where both the short-range and the long-range contributions to the interaction are regularized in momentum space. Compared with the SCS regularized interactions, the new SMS regularized interactions remove three redundant short-range operators at N^3LO and use the most up-to-date values of the pion-nucleon low-energy constants from the Roy-Steiner equation analysis of Refs. [13,14]. Another feature of the SMS regularized interactions is that the highest chiral order, referred to as N^4LO+, includes four sixth-order contact interactions in F waves in order to precisely describe the neutron-proton F-wave phase shifts, which are still not converged at N^4LO. These SMS regularized chiral interactions have also been successfully applied to *ab initio* calculations of the nuclear structure and reactions [15–21].

However, as a new generation of high-precision *NN* interaction, the chiral EFT interactions have rarely been used to investigate the pairing properties of nuclear matter, which is important to understand the properties of nuclear interactions and improve nuclear many-body calculations. Especially, the pairing correlations in the coupled channels, such as $^3SD_1$ and $^3PF_2$, may shed light on the properties of the tensor components of *NN* interaction. In addition, the reliable knowledge of

*shangxinle@impcas.ac.cn

the pairing gap itself in nuclear matter is key to understanding various phenomena in compact star physics, such as the cooling of new born stars [22], the afterburst relaxation in x-ray transients [23], and the glitches [24,25]. We therefore study in this work the pairing properties of the above-addressed chiral EFT interactions in nuclear matter within the BCS approximation. Specifically, we focus on the pairing properties in the $^1S_0$, $^3SD_1$, and $^3PF_2$ channels, which are supposed to be the dominant superfluid channels [26]. We use a free single-particle spectrum where the only uncertainty of pairing gaps stems from the *NN* interactions adopted. Therefore, these investigations may reveal essentially the properties of *NN* interactions themselves. We defer to include more realistic medium polarization effects in the future, where the self-energy [27] of nucleons (i.e., the effects of nucleon effective mass [28–30] and quasiparticle strength [31–34]) and vertex corrections [35] in pairing interaction are embodied.

II. THEORY AND DISCUSSION

Within the BCS approximation, the pairing gap is determined by the following gap equation:

$$\begin{pmatrix}\Delta_L(k)\\ \Delta_{L+2}(k)\end{pmatrix} = -\frac{1}{\pi}\int dk' k'^2 \begin{pmatrix}V_{L,L}(k,k') & V_{L,L+2}(k,k')\\ V_{L+2,L}(k,k') & V_{L+2,L+2}(k,k')\end{pmatrix} \times \frac{1}{\sqrt{\xi_{k'}^2 + D^2(k')}}\begin{pmatrix}\Delta_L(k')\\ \Delta_{L+2}(k')\end{pmatrix}, \tag{1}$$

with

$$D^2(k) = \Delta_L^2(k) + \Delta_{L+2}^2(k), \tag{2}$$

$$\xi_k = \tfrac{1}{2}\left(\varepsilon_k^a + \varepsilon_k^b\right), \tag{3}$$

where $\varepsilon_k^{a/b} = \frac{k^2}{2m} - \mu_{a/b}$ (with $\mu_{a/b}$ denoting the chemical potential) corresponds to the single-particle energy of the two pairing nucleons. Specifically, we use $\mu_n = \mu_p = \mu_a = \mu_b = \mu$ for the $^3SD_1$ neutron-proton pairing in symmetric nuclear matter, neglecting the difference between protons and neutrons, while $\mu_a = \mu_b = \mu_n = \mu$ for the $^1S_0$ and $^3PF_2$ neutron-neutron pairing in pure neutron matter. Due to the tensor force, the neutron-proton (neutron-neutron) pairing in the $^3SD_1$ ($^3PF_2$) channel is in the coupled channel. The nondiagonal element $V_{L,L+2}$ contains the main contributions of the tensor force and vanishes for neutron-neutron pairing in the $^1S_0$ channel. The corresponding gap equation for the $^1S_0$ channel reduces to a 1×1 dimension. We address here that for non-*S*-wave pairing ($^3SD_1$ and $^3PF_2$) the equivalent pairing gap $D^2(\mathbf{k})$ is substantially anisotropic and complicated [36]. Since the anisotropic pairing gap becomes important only in the asymmetric case [37,38], we adopt the angle-averaging procedure [39], i.e., $D^2(\mathbf{k}) \to D^2(k) = \frac{1}{4\pi}\int d\Omega_{\mathbf{k}} D^2(\mathbf{k}) = \Delta_L^2(k) + \Delta_{L+2}^2(k)$, for the $^3SD_1$ and $^3PF_2$ pairing gaps in the present work. In nuclear matter, the gap equation should be solved simultaneously with the density constraint

$$\rho_{a/b} = \int \frac{d^3k}{(2\pi)^3}\left(1 - \frac{\xi_k}{\sqrt{\xi_k^2 + D^2(k)}}\right), \tag{4}$$

to determine the pairing gaps $\Delta_L(k)$ and $\Delta_{L+2}(k)$ and the chemical potential μ at a given density ρ. Considering the pairing gap turns out to be important only near the chemical potential (corresponding to $\xi_k = 0$), we hereafter refer to the pairing gap as

$$\Delta_F = D(k_F), \tag{5}$$

with $\xi_{k_F} = 0$ (or equivalently $k_F = \sqrt{2m\mu}$ for a free single-particle spectrum). One should note that $k_F = \sqrt{2m\mu}$ is tending to $k_F = (3\pi^2\rho)^{1/3}$ $[(3\pi^2\rho/2)^{1/3}]$ for pure neutron matter (symmetric nuclear matter) when $D(k) \to 0$. To solve Eq. (1) numerically, we use the chiral interactions in the momentum space, i.e., $V_{L,L'}(k,k')$, for convenience.

In order to have a rough view of the pairing properties of the chiral interactions, we present in Fig. 1 the pairing properties of the SMS regularized chiral interactions in the $^3SD_1$ channel in symmetric nuclear matter and the $^1S_0$ and $^3PF_2$ channels in pure neutron matter. We calculate these pairing gaps using the BCS approximation from NLO up through N^{4}LO+ for regulators $\Lambda = 400$–550 MeV. We do not show the results for the LO interaction, which is much less accurate than the higher-order interactions. We find in Fig. 1 that the regular dependence of the $^3SD_1$ pairing gaps is weak at low densities and becomes apparent with the density increasing. The density dependence and regulator dependence of the pairing gaps in the $^1S_0$ and $^3PF_2$ channels in Fig. 1 are overall similar to those calculated with the SCS regularized interactions in Ref. [40] for the same chiral order from LO to N^{4}LO, since the regulations in momentum space and in coordinate space can be approximately correlated via $\Lambda \sim \frac{1}{R}$. One of the exceptions, in contrast to the SCS case, is that the sensitivity of the $^1S_0$ gaps to the regulator Λ becomes rather weak starting from N^{3}LO and almost invisible at N^{4}LO and N^{4}LO+ due to the removal of the redundant contact terms in these SMS regularized chiral interactions. Similar regulator dependence was found in Ref. [10] for the equation of states in symmetric nuclear matter and neutron matter calculated with the SCS regularized interactions. These complicated regulator dependence patterns may stem from different ranges of *NN* interactions or interplay of interactions at different ranges.

In Fig. 2, we investigate the convergence of the pairing gaps in the $^3SD_1$, $^1S_0$, and $^3PF_2$ channels with respect to the chiral order employing the SCS and SMS regularized chiral interactions, with regulators $R = 0.9$ fm and $\Lambda = 450$ MeV, respectively. Each of them corresponds to one of the most accurate regularizations found in Refs. [2,3,12]. We also present the results of the Argonne v18 (Av18) potential [41] for comparison.

We find in Fig. 2(a) that the $^3SD_1$ gaps tend to convergence at N^{3}LO for the SCS regularized chiral interactions. However, the results calculated with the most accurate N^{4}LO interaction diverge from the Av18 results at high densities, which indicates that the *NN* interaction in the $^3SD_1$ channel

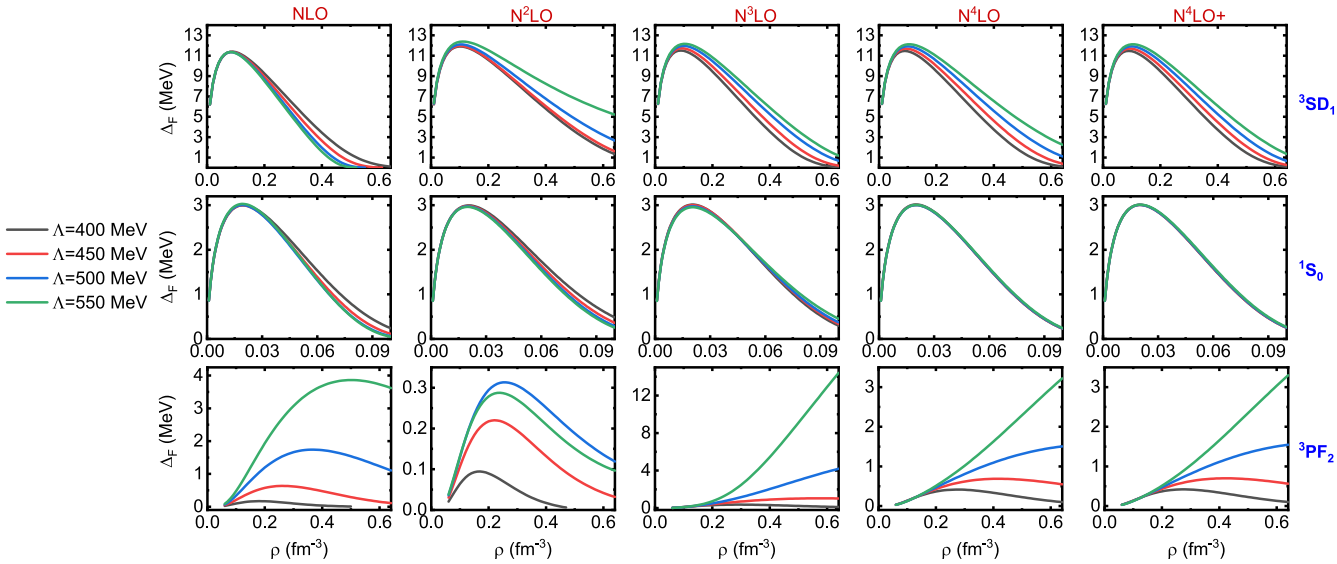

FIG. 1. Pairing gaps in the ${}^3SD_1$ channel in symmetric nuclear matter (upper panels) and pairing gaps in the ${}^1S_0$ (middle panels) and ${}^3PF_2$ (lower panels) channels in neutron matter calculated with the SMS regularized chiral *NN* interactions from NLO up through N^{4}LO+ for regulators $\Lambda = 400$–550 MeV.

at high scattering energy might need to be further constrained. We find in Fig. 2(b) that the ${}^1S_0$ gaps are very close for all the SCS regularized interactions. The ${}^1S_0$ gaps show apparent convergence pattern with respect to the chiral order and the N^{4}LO results are very close to the Av18 results, which may be due to the *NN* phase shift in the ${}^1S_0$ being well constrained for different potentials. In Fig. 2(c) we notice that the SCS regularized chiral interactions predict different ${}^3PF_2$ gaps at even rather low densities. We observe a convergence trend for the results calculated with the chiral interactions from N^{3}LO to N^{4}LO at low densities, and the converged results are consistent with the Av18 results since these three interactions describe reasonably the *NN* phase shifts in the ${}^3PF_2$ channel (regardless of F wave) for scattering energies up to 300 MeV. However, the convergence trend is broken at high densities, indicating that we may need higher chiral orders to reach convergence for the ${}^3PF_2$ pairing gaps. A similar convergence pattern of the ${}^3PF_2$ pairing gaps was observed in Ref. [40] for local chiral interactions from LO to N^{2}LO. Our results for the SCS regularized interactions are exactly the same as those in Ref. [40] calculated with a free spectrum approximation.

In panels (d)–(f) of Fig. 2 we observe chiral order dependencies of the ${}^3SD_1$, ${}^1S_0$, and ${}^3PF_2$ pairing gaps for the SMS

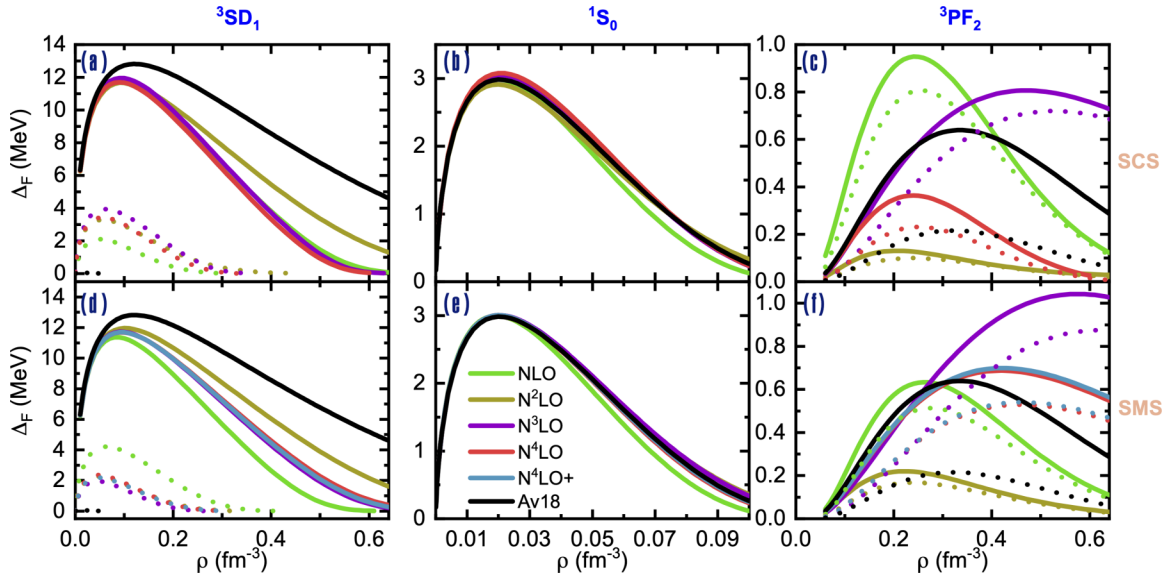

FIG. 2. Pairing gaps (solid lines) in the ${}^3SD_1$ [panels (a) and (d)], ${}^1S_0$ [panels (b) and (e)], and ${}^3PF_2$ [panels (c) and (f)] channels calculated with the Av18 potential and chiral *NN* interactions. Upper (lower) panels show the results of the SCS (SMS) regularized interactions from NLO up through N^{4}LO (N^{4}LO+) with the same regulator $R = 0.9$ fm ($\Lambda = 450$ MeV). The contributions of the ${}^3S_1$ [panels (a) and (d)] and ${}^3P_2$ [panels (c) and (f)] single channels to the pairing gaps of the coupled ${}^3SD_1$ and ${}^3PF_2$ channels are represented by the dotted lines.

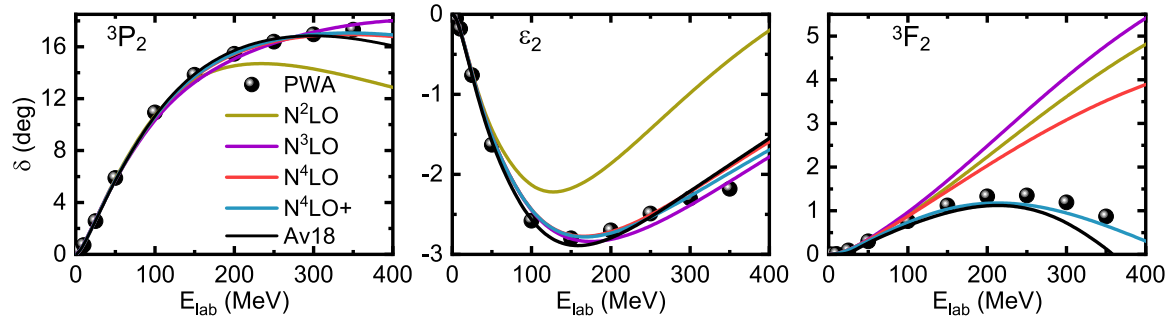

FIG. 3. Neutron-proton phase shifts in the $^3P_2$ and $^3F_2$ channels and the mixing parameter ε_2 as functions of the scattering energy $E_{\rm lab}$ predicted with the SMS regularized chiral interactions (from N^{2}LO to N^{4}LO+) and the Av18 potential (solid lines). The results from the Nijmegen partial-wave analysis [46] (solid dots) are shown for comparison.

regularized chiral interactions similar to the dependencies in panels (a)–(c) for the SCS regularized chiral interactions from NLO to N^{4}LO. We find in panels (d)–(f) that the $^3SD_1$, $^1S_0$, and $^3PF_2$ pairing gaps for the N^{4}LO and N^{4}LO+ interactions are rather close. Though the leading F-wave contact interactions of the N^{5}LO level introduced in the N^{4}LO+ interaction have a small effect on the $^3PF_2$ pairing gaps, one may need a complete N^{5}LO interaction to assess the convergence pattern of the $^3PF_2$ pairing gaps in a more conclusive way.

The parameters of *NN* interactions adopted in this work are obtained via different fitting procedures. Therefore, their off-shell constituents could be quite different though their on-shell properties have been well constrained by the same *NN* scattering phase shifts. These difference might be revealed in their predictions of various nuclear properties. For example, the D-wave probabilities of the deuteron calculated with these interactions are apparently different [2,3,12,41]. In order to investigate the detailed constituents of these interactions, especially the tensor force components, we show in Fig. 2 the pairing gaps of the $^3S_1$ (and $^3P_2$) single channel (dotted lines), which are calculated by considering only the $^3S_1$ (and $^3P_2$) single channel in solving Eq. (1) as in the earlier investigation [42,43] [that is, we remove the $V_{L,L+2}$ elements in Eq. (1)]. We emphasize that the calculations with all the adopted interactions predict the nonexistence of the pairing gaps in the $^3D_1$ and $^3F_2$ single channels.

As is well known, the $^3SD_1$ gap equation reduces to the Schrödinger equation for the deuteron bound state in the limit of vanishing density [44,45]. The accurate description of the adopted interactions of the deuteron binding energy ensures the similar behavior of the $^3SD_1$ pairing gaps at low densities in Fig. 2. However, it does not mean that the contributions of different components of *NN* interactions to the $^3SD_1$ pairing gaps are similar. Actually, the discrepancies of the $^3S_1$ pairing gap among different interactions (especially the distinction between chiral interaction and Av18 potential) are remarkable, which indicates the tensor force components of these interactions in the $^3SD_1$ channel are different, as expected. The differences of the tensor force effects for these interactions become more significant at higher densities. One of the common features of the chiral interactions (regardless of the inaccurate LO interactions) and the Av18 potential is the contributions of the tensor force components are much more important than the $^3S_1$ single channel. Similarly, we find significant distinctions of the tensor force effects for the adopted interactions in the $^3PF_2$ channel [see Figs. 2(c) and 2(f)]. Therefore, the tensor force components of these interactions in the $^3PF_2$ channel are also different. Unlike with the results in the $^3SD_1$ channel, the tensor force effects are less important than the $^3P_2$ single channel for the chiral interactions, while it is opposite for the Av18 potential in the $^3PF_2$ channel.

In order to analyze the large spread of the $^3PF_2$ pairing gaps in Fig. 2 [panel (c), for example] at high densities, we present in Fig. 3 the neutron-proton phase shifts in this channel. We find in Fig. 3 that the SMS regularized N^{2}LO interaction is not well constrained by the phase shifts at even low scattering energies. Therefore, the $^3PF_2$ pairing gap of the N^{2}LO interaction is quite different from the results of other more accurate interactions at even low densities as shown in Fig. 2(c). We notice in Fig. 3 that the N^{4}LO interaction is much less accurate in describing the $^3F_2$ phase shift compared to the improved N^{4}LO+ interaction. However, the $^3PF_2$ pairing gaps in Fig. 2(c) calculated with these two interactions are nearly the same. Therefore, the interaction in the $^3F_2$ channel has nearly no effects on the $^3PF_2$ pairing gaps, and the large spread of the $^3PF_2$ pairing gaps in Fig. 2(c) (solid lines) at high densities may stem mainly from the difference of interactions in the $^3P_2$ channel and the coupling of $^3P_2$ and $^3F_2$. Both the Av18 potential and the N^{4}LO+ chiral interaction provide good descriptions for the $^3P_2$ phase shifts and the mixing parameter ε_2 below $E_{\rm lab} = 300$ MeV as shown in Fig. 3. Accordingly, the $^3PF_2$ pairing gaps calculated with these two interactions in Fig. 2(c) are overall close to each other from low to intermediate densities. However, the contributions of the $^3P_2$ channel [dotted lines in Fig. 2(c)] behave quite differently for these two interactions starting from low densities. Therefore, the detailed constitutes of *NN* interactions could be very different though they provide similar descriptions for the phase shifts.

In Fig. 4 we estimate the truncation errors of chiral expansion for the pairing gaps calculated by the SMS regularized interactions using a Bayesian approach with the degree-of-belief intervals of 1σ and 2σ (see Appendix A for details). Since the N^{4}LO+ interaction is not a complete N^{5}LO interaction, we do not evaluate the truncation errors of pairing gaps at N^{4}LO+. From NLO to N^{4}LO, the truncation errors of the $^3SD_1$ and $^1S_0$ gaps decease systematically

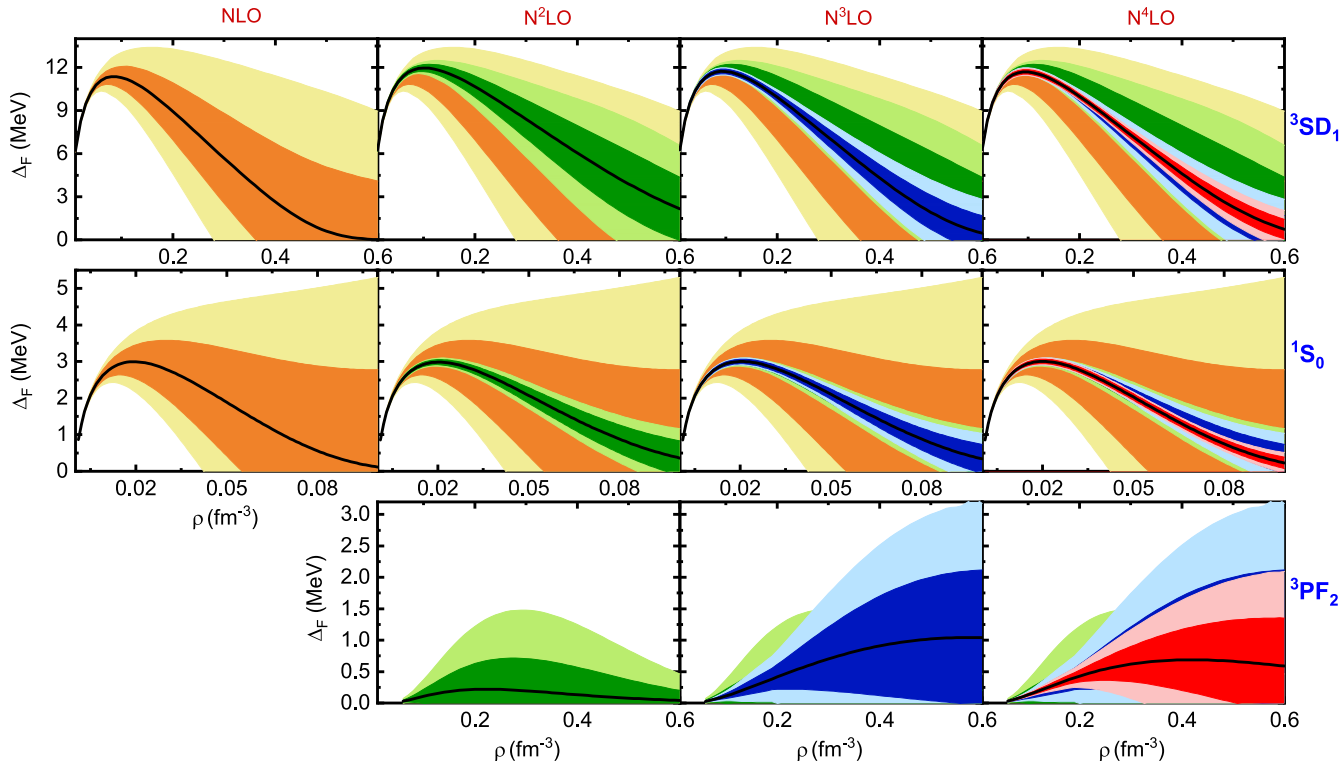

FIG. 4. Pairing gaps with truncation errors in the ${}^3SD_1$, ${}^1S_0$, and ${}^3PF_2$ channels calculated by the SMS regularized chiral *NN* interactions with regulator $\Lambda = 450$ MeV from LO up through N^{4}LO. The dark-shaded band for each color indicates the 1σ degree-of-belief interval, while the light-shaded bands correspond to 2σ standard deviation.

order by order. The truncation errors become rather small at N^{4}LO in particular. These calculations demonstrate that the chiral potentials in these two channels present rather good convergence for the current application. The truncation errors of the ${}^3PF_2$ gaps decrease also systematically order by order at low densities. However, such a systematic evolution is broken as the density increases, though the truncation errors at N^{3}LO and N^{4}LO are of comparable size. It indicates that we may need higher chiral orders to reach convergence in this channel as we point out in Fig. 2. The truncation errors of chiral expansion for the ${}^1S_0$ and ${}^3PF_2$ gaps calculated with the SCS regularized interactions have been investigated in Ref. [40] with an easily operational analysis methodology proposed in Refs. [2,3]. These evaluations neglect the LO contributions to the higher-order uncertainties, and a term ensuring that the next order always lies within the uncertainty band of the previous order, in contrast to Refs. [2,3]. Therefore, the systematic evolution of the truncation errors for the ${}^1S_0$ gaps with the chiral order we observe in Fig. 2 was not found in Ref. [40]. The systematic evolution of the truncation errors for the ${}^3PF_2$ gaps with the chiral order at low densities we observe in Fig. 2 was also not found in Ref. [40]. We are consistent with Ref. [40] that the uncertainties are very small for the ${}^1S_0$ channel but sizable for the ${}^3PF_2$ channel. We find similar behavior for the truncation errors obtained with the SCS regularized interactions (see Appendix B for details).

We emphasize that we investigate the pairing properties of the two-nucleon forces and do not include the contributions of three-nucleon forces in this work. The pairing gaps and the truncation errors starting from N^{2}LO are incomplete and should be revisited once the calculations with the three-nucleon forces become available. The results at N^{2}LO and beyond obtained in this work may reveal a potentially achievable accuracy at the corresponding chiral orders.

III. CONCLUSIONS AND OUTLOOK

In conclusion, we investigated the pairing properties of state-of-the-art SCS and SMS regularized chiral EFT interactions in nuclear matter within the BCS approximation. Specifically, we calculated the pairing gaps in the ${}^3SD_1$, ${}^1S_0$, and ${}^3PF_2$ channels.

We investigated the regulator dependence and the chiral-order convergence pattern of pairing gaps. The ${}^3SD_1$ and ${}^1S_0$ pairing gaps show overall weak regulator dependence and robust convergence from low to high densities, while the ${}^3PF_2$ results show chaotic behavior. The truncation errors evaluated with the Bayesian approach present similar features for these channels. Comparing the converged results of the chiral interactions with those of the Av18 potential, we found they coincide with each other at low densities for all of these three channels. However, we observed an apparent discrepancy in the results of the chiral interaction and Av18 potential in the ${}^3SD_1$ and ${}^3PF_2$ channels at high densities, indicating the *NN* interactions in these two channels may need further constraints at high scattering energies in the future.

In addition, we have investigated the effect of the tensor force on the ${}^3SD_1$ and ${}^3PF_2$ pairing gaps with the Av18 potential and the chiral interactions. We found significant

differences of the tensor force effects for the $^3SD_1$ and $^3PF_2$ pairing gaps, indicating that the tensor components in these interactions are quite different. One of the common features of the chiral interactions (regardless of the inaccurate LO interactions) and the Av18 potential is the contribution of the tensor force components are overall more important than the $^3S_1$ single channel. In contrast to the $^3SD_1$ channel, the tensor force effects are less important than the $^3P_2$ single channel for the chiral interactions, while it is the opposite for the Av18 potential in the $^3PF_2$ channel.

The pairing gaps obtained in this work can be applied to compact star physics only if the medium effects are included. We use a free single-particle spectrum in this work since we focus solely on investigating the properties of the *NN* interactions themselves. Besides, the results in this work are obtained with only the two-body interactions. Including three-body force (3BF) may change our conclusions. The expressions for the chiral 3BF have been worked out completely up to N^{3}LO. We will include the chiral 3BF in nuclear many-body calculations and investigate the effects of the 3BF on the pairing correlations in nuclear matter, which is challenging in numerical implementations. Employing self-consistent 2BF and 3BF, we will be able to study the effect of the pairing correlations in the neutron star cores on the neutron star cooling phenomena.

ACKNOWLEDGMENTS

This work was supported by the National Natural Science Foundation of China under Grants No. 11975282, and No. 12375117; the Youth Innovation Promotion Association of Chinese Academy of Sciences (Grant No. Y2021414) the Strategic Priority Research Program of Chinese Academy of Sciences under Grant No. XDB34000000; the Key Research Program of the Chinese Academy of Sciences under Grant No. XDPB15; the DFG and NSFC through funds provided to the Sino-German CRC 110 "Symmetries and the Emergence of Structure in QCD" (NSFC Grant No. 12070131001, Project ID 196253076-TRR110); the ERC AdG Nuclear Theory under Grant No. 885150; and the Gansu Natural Science Foundation under Grant No. 23JRRA675.

APPENDIX A: BAYESIAN ANALYSIS

We use the Bayesian scheme of Refs. [47,48] to estimate the truncation errors of pairing gaps from chiral potentials. The generic assumption is that a nuclear observable X in chiral EFT can be expanded with a dimensionless parameter Q as follows:

$$X = X_{\rm ref} \sum_{n=0}^{\infty} c_n Q^n, \tag{A1}$$

where $X_{\rm ref}$ is the natural size of X and c_ns are dimensionless parameters. In this work, we investigate the truncation errors of the pairing gap Δ_F in nuclear matter. Therefore, the observable X is Δ_F and the expansion parameter is regarded as $Q = \frac{k_F}{\Lambda_b}$, with k_F being the Fermi momentum of the nucleon determined by the nuclear density ρ and Λ_b being the chiral EFT breakdown scale. We take $\Lambda_b = 700$ MeV, which is much higher than the maximum Fermi momentum 515 MeV (corresponding to $\rho = 0.6$ fm^{-3} for pure neutron matter) in this work.

The error of the observable truncated at the order k of the expansion is defined as $X_{\rm ref}\Delta_k$, with the dimensionless function Δ_k calculated by

$$\Delta_k = \sum_{n=k+1}^{\infty} c_n Q^n. \tag{A2}$$

In practice, we sum over n up to $h + k + 1$ order and neglect the higher orders. The coefficients c_n, with $n \geqslant k+1$, are extracted by the known expansion coefficients c_n, with $n \leqslant k$. In the Bayesian model, we define a probability distribution function (pdf) for Δ_k as $pr_h(\Delta|\boldsymbol{c_k})$, determined by a vector composed of lower coefficients, $\boldsymbol{c_k} \in \{c_2, c_3, \ldots, c_k\}$. The subscript h means only h higher terms are included in the truncation error, which is 10 in this work. Note that $\boldsymbol{c_k}$ does not include c_0 and c_1, since c_0 is dependent on the natural size of X and $c_1 = 0$ is required by the symmetry in chiral EFT.

The pdf determines the degree-of-belief p, with the highest posterior density, as

$$p = \int_{-d_k^{(p)}}^{d_k^{(p)}} pr_h(\Delta|\boldsymbol{c_k}) d\Delta, \tag{A3}$$

where $(100 \times p)\%$ is the probability for the true value of the nuclear observable X staying in $\pm X_{\rm ref} d_k^{(p)}$ at the $(k+1)$ order (N^{k}LO) prediction.

In Ref. [47], Δ_k was derived in terms of the expansion coefficients c_n's by assuming them to be random variables drawn from a shared distribution centered at zero with a characteristic size or upper bound $\bar{c}$. The pdf function can be written with the Bayesian theorem as

$$pr_h(\Delta|\boldsymbol{c_k}) = \frac{\int_0^\infty d\bar{c} pr_h(\Delta|\bar{c}) pr(\bar{c}) \prod_{n=2}^k pr(c_n|\bar{c})}{\int_0^\infty d\bar{c} pr(\bar{c}) \prod_{n=2}^k pr(c_n|\bar{c})}, \tag{A4}$$

where we use the following priors:

$$pr(c_n|\bar{c}) = \frac{1}{2\bar{c}} \theta(\bar{c} - |c_n|), \tag{A5}$$

$$pr(\bar{c}) = \frac{1}{\sqrt{2\pi}\bar{c}\sigma} e^{-(\ln \bar{c})^2/2\delta^2}.$$

The prior $pr_h(\Delta|\bar{c})$ can be worked out with

$$pr_h(\Delta|\bar{c}) = \frac{1}{2\pi} \int_{-\infty}^{\infty} dt \cos(\Delta t) \prod_{i=k+1}^{k+h} \frac{\sin(\bar{c}Q^i t)}{\bar{c}Q^i t}. \tag{A6}$$

With the above equations, we can obtain $d_k^{(p)}$ in Eq. (A3) numerically as an inversion problem.

In this work, we take $X_{\rm ref}$ to be Δ_F of the LO interactions for the $^3SD_1$ and $^1S_0$ channels. Since we find nonexistence of $^3PF_2$ pairing gaps for the LO interactions, we take $X_{\rm ref}$ to be Δ_F/Q^2 of the NLO interactions in this channel.

APPENDIX B: TRUNCATION ERRORS OF PAIRING GAPS WITH THE SCS REGULARIZED INTERACTIONS

Figure 5 shows the truncation errors of pairing gaps with the SCS regularized interactions.

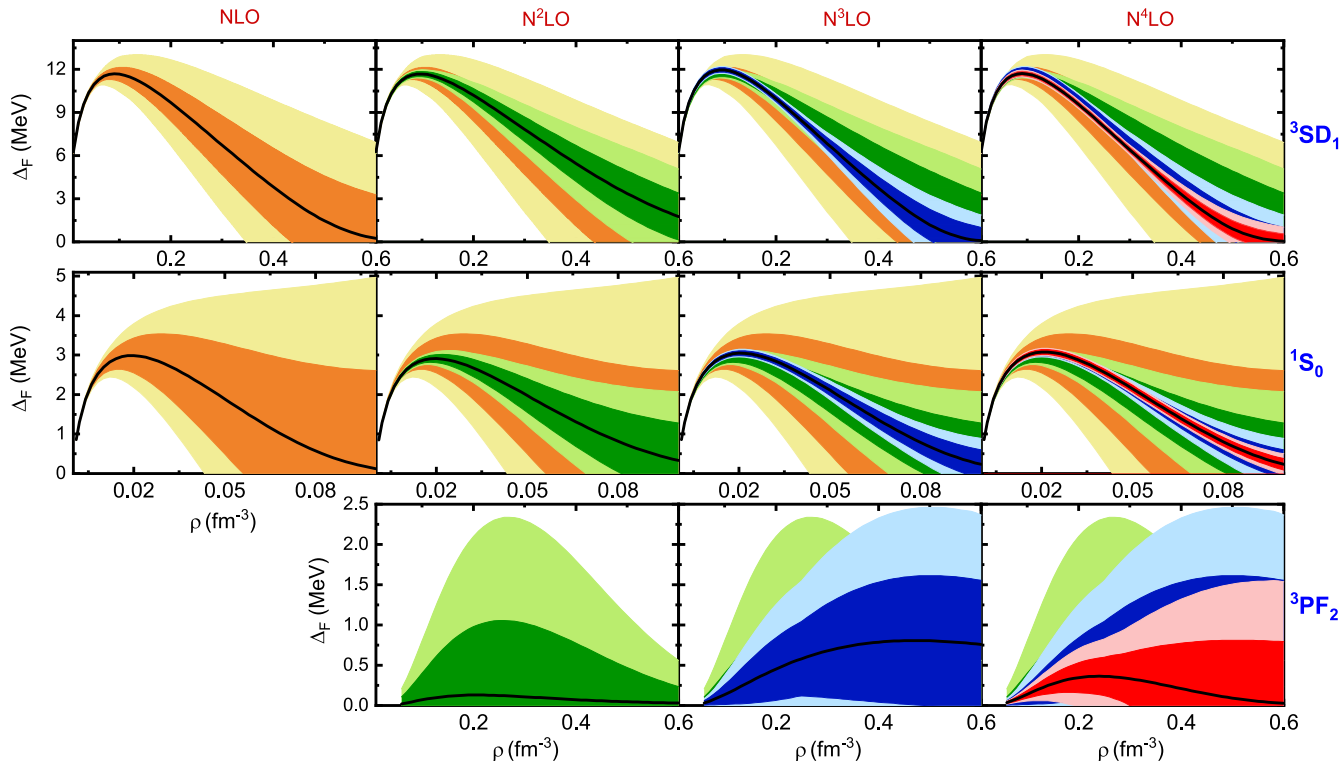

FIG. 5. Pairing gaps with truncation errors in the ${}^3SD_1$, ${}^1S_0$, and ${}^3PF_2$ channels calculated by the SCS regularized chiral *NN* interactions with regulator $\lambda = 0.9$ fm from LO up through N^{4}LO. The dark-shaded band for each color indicates the 1σ degree-of-belief interval, while the light-shaded bands correspond to 2σ standard deviation.

[1] E. Epelbaum, H. W. Hammer, and U.-G. Meißner, Rev. Mod. Phys. **81**, 1773 (2009).
[2] E. Epelbaum, H. Krebs, and U.-G. Meißner, Eur. Phys. J. A **51**, 53 (2015).
[3] E. Epelbaum, H. Krebs, and U.-G. Meißner, Phys. Rev. Lett. **115**, 122301 (2015).
[4] S. Binder *et al.* (LENPIC Collaboration), Phys. Rev. C **93**, 044002 (2016).
[5] P. Maris, S. Binder, A. Calci, E. Epelbaum, R. J. Furnstahl, J. Golak, K. Hebeler, H. Kamada, H. Krebs, and J. Langhammer *et al.*, EPJ Web Conf. **113**, 04015 (2016).
[6] S. Binder *et al.* (LENPIC Collaboration), Phys. Rev. C **98**, 014002 (2018).
[7] P. Yin, W. Du, W. Zuo, X. Zhao, and J. P. Vary, J. Phys. G: Nucl. Part. Phys. **49**, 125102 (2022).
[8] W. Du, S. Pal, M. Sharaf, P. Yin, S. Sarker, A. M. Shirokov, and J. P. Vary, Phys. Rev. C **106**, 054608 (2022).
[9] P. Yin, W. Du, W. Zuo, X. Zhao, and J. P. Vary, arXiv:2208.00267.
[10] J. Hu, Y. Zhang, E. Epelbaum, U.-G. Meißner, and J. Meng, Phys. Rev. C **96**, 034307 (2017).
[11] J. Hu, P. Wei, and Y. Zhang, Phys. Lett. B **798**, 134982 (2019).
[12] P. Reinert, H. Krebs, and E. Epelbaum, Eur. Phys. J. A **54**, 86 (2018).
[13] M. Hoferichter, J. Ruiz de Elvira, B. Kubis, and U.-G. Meißner, Phys. Rev. Lett. **115**, 192301 (2015).
[14] M. Hoferichter, J. Ruiz de Elvira, B. Kubis, and U.-G. Meißner, Phys. Rep. **625**, 1 (2016).
[15] E. Epelbaum, J. Golak, K. Hebeler, H. Kamada, H. Krebs, U.-G. Meißner, A. Nogga, P. Reinert, R. Skibiński, and K. Topolnicki *et al.*, Eur. Phys. J. A **56**, 92 (2020).
[16] Y. Volkotrub, J. Golak, R. Skibiński, K. Topolnicki, H. Witała, E. Epelbaum, H. Krebs, and P. Reinert, J. Phys. G: Nucl. Part. Phys. **47**, 104001 (2020).
[17] V. Urbanevych, R. Skibiński, H. Witała, J. Golak, K. Topolnicki, A. Grassi, E. Epelbaum, and H. Krebs, Phys. Rev. C **103**, 024003 (2021).
[18] A. A. Filin, V. Baru, E. Epelbaum, H. Krebs, D. Möller, and P. Reinert, Phys. Rev. Lett. **124**, 082501 (2020).
[19] A. A. Filin, D. Möller, V. Baru, E. Epelbaum, H. Krebs, and P. Reinert, Phys. Rev. C **103**, 024313 (2021).
[20] P. Maris, E. Epelbaum, R. J. Furnstahl, J. Golak, K. Hebeler, T. Hüther, H. Kamada, H. Krebs, U.-G. Meißner, J. A. Melendez, A. Nogga, P. Reinert, R. Roth, R. Skibinski, V. Soloviov,

K. Topolnicki, J. P. Vary, Y. Volkotrub, H. Witala, and T. Wolfgruber (LENPIC Collaboration), Phys. Rev. C **103**, 054001 (2021).
[21] P. Maris *et al.* (LENPIC Collaboration), Phys. Rev. C **106**, 064002 (2022).
[22] J. M. Lattimer, K. A. van Riper, M. Prakash, and M. Prakash, Astrophys. J. **425**, 802 (1994).
[23] D. Page and S. Reddy, in *Neutron Stars Crust*, edited by C. Bertulani and J. Piekarewicz (Nova, Hauppauge, NY, 2012), pp. 281–308.
[24] J. Piekarewicz, F. J. Fattoyev, and C. J. Horowitz, Phys. Rev. C **90**, 015803 (2014).
[25] X. Shang and A. Li, Astrophys. J. **923**, 108 (2021).
[26] U. Lombardo, H. Schulze, C. W. Shen, and W. Zuo, Int. J. Mod. Phys. E **14**, 513 (2005).
[27] X. H. Fan, X. L. Shang, J. M. Dong and W. Zuo, Phys. Rev. C **99**, 065804 (2019).
[28] J. W. Holt, N. Kaiser, and W. Weise, Nucl. Phys. A **876**, 61 (2012).
[29] J. W. Holt, N. Kaiser, and T. R. Whitehead, Phys. Rev. C **97**, 054325 (2018).
[30] X. L. Shang, A. Li, Z. Q. Miao, G. F. Burgio, and H. J. Schulze, Phys. Rev. C **101**, 065801 (2020).
[31] M. Baldo, U. Lombardo, H. J. Schulze, and Z. Wei, Phys. Rev. C **66**, 054304 (2002).
[32] P. Bożek, Phys. Lett. B **551**, 93 (2003).
[33] M. Baldo and A. Grasso, Phys. Lett. B **485**, 115 (2000).
[34] U. Lombardo, P. Schuck, and W. Zuo, Phys. Rev. C **64**, 021301(R) (2001).
[35] W. Guo, U. Lombardo, and P. Schuck, Phys. Rev. C **99**, 014310 (2019).
[36] X. L. Shang and W. Zuo, Phys. Rev. C **88**, 025806 (2013).
[37] X. L. Shang, P. Wang, W. Zuo, and P. Yin, J. Phys. G: Nucl. Part. Phys. **42**, 055105 (2015).
[38] L. Zhang, J. B. Wang, X. L. Shang, and Y. Gao, New J. Phys. **24**, 103006 (2022).
[39] M. Baldo, I. Bombaci, and U. Lombardo, Phys. Lett. B **283**, 8 (1992).
[40] C. Drischler, T. Krüger, K. Hebeler, and A. Schwenk, Phys. Rev. C **95**, 024302 (2017).
[41] R. B. Wiringa, V. G. J. Stoks, and R. Schiavilla, Phys. Rev. C **51**, 38 (1995).
[42] L. Amundsen and E. Østgaard, Nucl. Phys. A **442**, 163 (1985).
[43] M. Baldo, J. Cugnon, A. Lejeune, and U. Lombardo, Nucl. Phys. A **536**, 349 (1992).
[44] M. Baldo, U. Lombardo, and P. Schuck, Phys. Rev. C **52**, 975 (1995).
[45] U. Lombardo, P. Nozieres, P. Schuck, H. J. Schulze, and A. Sedrakian, Phys. Rev. C **64**, 064314 (2001).
[46] V. G. J. Stoks, R. A. M. Klomp, M. C. M. Rentmeester, and J. J. de Swart, Phys. Rev. C **48**, 792 (1993).
[47] R. J. Furnstahl, N. Klco, D. R. Phillips, and S. Wesolowski, Phys. Rev. C **92**, 024005 (2015).
[48] J. A. Melendez, S. Wesolowski, and R. J. Furnstahl, Phys. Rev. C **96**, 024003 (2017).